BioBacta

Journal of Medical and Life Science
https://jmals.journals.ekb.eg/

Anti-tumor Activity of Gold nanoparticles by Use High Content Screening Technique (HCS)

Ali G. Al-Dulimi[a]; Ahmed F. Hasan[b]; Osama A. Al–Mogadamy[c]

[a] Department of Dentistry, Al-Farabi University College (FUC), Al-Dora Square, Al-Masafee Street, Baghdad, Iraq

[b] Department of Biology, Al-Farabi University College (FUC), Al-Dora Square, Al-Masafee Street, Baghdad, Iraq

[c] Diyala Health Directorate, Ministry of Health, Iraq.

Correspondence should be addressed to the following author:

E-mail: ahmedfalih@alfarabiuc.edu.iq **Tel.:** +964 (0) 7707347902.

DOI: 10.21608/jmals.2022.256487

Abstract

Gold nanoparticles (GNPs) act as less toxic and effective drug carriers with many specific properties that are particularly useful for biomedical and pharmaceutical applications. The present study was conducted to determine the anti-tumor properties GNPs. The new preparation technique is quick and cost-effective. GNPs formation was confirmed using various characterization techniques including X-Ray diffraction (XRD) analysis, field emission scanning electron microscopy (FE-SEM), energy dispersive X-ray spectrometer (EDX), and transmission electron microscopy (TEM). XRD, FES-EM, and TEM experiments have confirmed the formation of GNPs which shows that the prepared particles are spherical inform and have a smooth surface with an average size of 24.32 ± 1.32 nm. Multiparametric analysis of GNPs toxicity at the level of individual cells using flow cytometry and cellular imaging-based approaches such as High Content Screening (HCS) have played key roles in the detection of toxicity and classification of compounds based on observed patterns of reversible and irreversible cellular injury. The effect of GNPs on the MCF-7 cell line regarding cell viability, cell nucleus morphology, membrane permeability, potential mitochondrial permeability, and cytochrome C release was further confirmed using a High Content Screening array scan via multi-parametric kit. Results indicated that the viable count of MCF-7 cells was highly decreased by treated with GNPs. Nuclei stained with Hoechst blue appeared to be mostly condensed in response to the treatment with the GNPs (1.5- fold increase in nuclear fluorescence intensity), with significant differences ($p < 0.0263$) as compared with untreated cells. Cell membrane permeability was significantly ($p = 0.0019$) upon GNPs showing an increase of 1.9-fold, as compared with the untreated MCF-7 cells. GNPs induce a significant ($p = 0.0053$) decrease in mitochondrial membrane potential by 32.7%, in comparison to the untreated cancer cells with significant induction of the release of cytochrome C ($p = 0.0016$) was recorded after exposure to the GNPs (0.43-fold increased mean intensity), The outcomes of the present study propose the high feasibility for using GNPs as a novel anticancer drug.

Keywords: Cell culture; Gold nanoparticles; HCS

Received: June 10, 2022; Accepted August 5, 2022; Published August 23, 2022

1. Introduction

Cancer is a predominant public health problem worldwide. More than eleven million people are identified with cancer every year. It is estimated that this number will be increased to sixteen million in the next years, with breast cancer keeping the rank of being the most frequent cancer and cause of death among women (1). The conventional therapies, including chemotherapy, radiation, and combination with surgery are not sufficiently effective, due to factors such as poor bio-distribution and non-specific delivery of chemotherapeutic drugs, high possibility of recurrence, limited therapeutic effectiveness, and undesired effects (2). For this reason, a crucial need for new, high-quality, and better-tolerated agents with chemotherapeutic activities, in addition to strategies for specific delivery of these agents to tumor cells. In the previous years, the majority of cancer treatment approaches made advantage of the systems of diagnosis and therapy that function based on nanotechnology. Most recent developments involved the multifunctional nanosystems conjugated to imaging probes and targeting factors that include, for instance, antibodies, aptamers, and enzymes (3). gold nanoparticles (GNPs) are a desirable delivering system of different anticancer drugs, as a result of having specific properties that include chemical resistivity, enzymatic stability, and low cytotoxicity. GNPs are also known to be biocompatible and easy to conjugate with other biologically active molecules such as Abs and enzymes. They also show particular optical properties, leading to an increased rate of binding to active groups such as amine and thiol and, thereby, an expanded possibility for modifying the cell surface (4). This study aims to investigate the potential therapeutic property of GNPs in breast cancer cells and to elucidate the molecular mechanism involved in the GNPs' antiproliferation of cancer cells. In this study, we reported the synthesis, characterization, and cytotoxic effect of GNPs on breast cancer cell lines (MCF7) was included in the cytotoxicity tests in comparison with doxorubicin (Doxorubicin has been used clinically as an antineoplastic drug in the treatment breast cancer) as a positive control. Morphological changes suggested the occurrence of apoptotic events.

2. Materials and Methods

A breast cancer cell line (MCF-7) was provided via the University of Malaya's Faculty of Medicine, Pharmacology department. Cellomics-Multiparametric Cytotoxicity 3 Kit (Thermo Scientific, USA) Antibiotics for example streptomycin and penicillin were made available (Bio-source International, Nivelles, Belgium). Other remainders were used in systematic grades.

2.1 Gold Nanoparticles (GNPs) Preparation

The GNPs were prepared following Al-Dulimi and his colleagues (5), with some modifications. GNPs with a diameter of 21 nm were created via heating of sodium citrate solution (100 mL) to 100°C and then adding 2 mL of HAuCl4. At 100°C. After 10 minutes, the solution's color changed to red wine, which indicates the creation of GNPs. After that, the solution was allowed to cool down to room temperature while being constantly stirred.

2.2 Characterization of Gold Nanoparticles

2.2.1 Field-Emission Scanning Electron Microscopic (FESEM)

The VEGA 3 (TESCAN, Czech Republic) SEM machine was used for the Field-Emission Scanning Electron Microscopic (FESEM) study. The morphology and nanoparticle grain size of the tested samples were visualized using FESEM. Thin films of GNPs reduce the quantity of solution on the cover slide, they were

created, and they were then allowed to dry at room temperature before being visualized under SEM. The analysis was carried out at Iraq's Ministry of Science and Technology's Department of Materials Research.

2.2.2 X-Ray Diffraction (XRD)

The crystallinity, metallic nature, and cubic structure of tested samples were determined using an XRD system (Phillips PW 1830) operating at a 40 kV voltage and a 20-mA current. The analysis was carried out at the Materials Research Department of Iraq's Ministry of Science and Technology.

2.2.3 Transmission Electron Microscopy (TEM)

The 400 kV JEOL JEM-1010 (JEOL Ltd., Japan) TEM system was used to capture the TEM images. The samples were dissolved in 90 percent ethanol and 30 minutes of sonication. Then, placed a drop of colloidal solution on a filter paper on a copper grid coated with a thin amorphous carbon film. Before being placed on the specimen holder, the samples were air-dried and vacuum-held in the desiccator. Nanomaterial particle size, composition, and distribution were all determined. The research was carried out at the Department of Medical Nanotechnology, Faculty of Advanced Technologies in Medicine, Iran University of Medical Sciences in Tehran, Iran.

2.2.4 High-content screening (HCS) assay

For further confirmation of toxicity on MCF-7 cells, high content screening (HCS) assay was performed to determine several parameters (e.g., cell viability, nuclear intensity, membrane permeability, MMP, and cytochrome c). After seeding of 1×10^{-5} MCF-7 cells in twelve-well plates, incubation was performed at 37 °C and 5% CO2 for 24 h. Then, the cells were treated with GNPs and compared with untreated cells (negative control) and cells treated with doxorubicin (positive control). After a period of incubation (24 h), MMP dye (Excitation 552/Emission 576) and the cell permeability dye (Excitation 491/Emission 509) were applied to the living cells which were subjected to another incubation for 1 h. Following fixation (4% formaldehyde, 15 min and permeabilization (0.1% Triton X- 100 in PBS). Then, the samples were subjected to blockage with 3% bovine serum albumin) and incubation with cytochrome c primary mouse antibody for 1 h. After washing three times using wash buffer I (16PBS), goat anti-mouse secondary antibodies conjugated with DyLightTM 649 were added. Then, wash buffer II (16PBS with 1% Tween-20) was used to rinse the cells. Finally, Hoechst 33 258 was applied to stain the nuclei while Cellomics ArrayScan HCS reader (Thermo Scientific) was employed for visualization. A cell health profiling bioapplication module was applied for the quantification of the fluorescence intensity of the dyes used (6).

3. Result and discussions

3.1 Preparation of Gold Nanoparticles

Gold nanoparticles (GNPs) of controlled size and shape have been synthesized using a variety of methods, including chemical, physical, and biological methods, and have had a significant medical impact on human health. As a result, gold salts are reduced by citrate to produce GNPs. Drop-by-drop addition of HAuCl4.3H2O. The color of the solution of boiling trisodium citrate dihydrate changed gradually from pale yellow to bluish grey, and red, indicating the formation of GNPs with a final concentration of 1 mg mL^{-1} (Fig. 1). Because of the citrate ions on the surface of GNPs have a negative charge, Citrate reduction is an advantageous strategy for preparing GNPs because GNPs disperse easily in polar solvents such as water (7). The emergence of the absorption band of localized resonance of surface plasmon (LSPR), which is distinctive of metal nanoparticles for example gold, was most likely responsible for the color shift. Furthermore, GNPs are relatively small particles in which the movement of electrons is restricted not as freely as they are in bulk gold. Because of this restriction in movement, Au particles react differently

to light sources (8). Colloidal suspensions of GNPs, for example, for larger spherical or nanorod particles, blue and purple are usual (Fig. 1B), and spherical particles less than 50 nm appear in a red color (Fig. 1C). The tiny spheres of GNPs with diameters ranging from 19 to 55 nm widely used to cancer treatment, allowing them to quickly infiltrate cancer cells and functionalize and interact with a wide range of chemicals. As a result, GNPs are recognized as the most efficient drug-carrier choice for treating many forms of cancer (9).

3.2 GNPs characterization

3.2.1 X-Ray diffraction (XRD) analysis

XRD was used to investigate the crystalline phase of GNPs. The findings of a structural investigation of GNPs using XRD are shown in Fig. (2). Bragg's reflections of 111; 200; 220; and 311 planes associated with the FCC (face-centered cubic) of GNPs are linked with strong diffraction peaks with two values at ($38.2^{o)}$; ($44.4^{o)}$; ($64.7^{o)}$; and ($77.7^{o)}$. The obtained diffraction peaks matched those that have been recorded for conventional gold metal Au^0. As a result, GNPs were primarily crystalline according to XRD indicated.

In the region of the GNPs distinctive peaks, a few intense extra and yet unselected peaks were also found. These peaks could have been caused by some intermediate compounds through the process of synthesis. The appearance of these unselected external peaks had no influence on the gold-specific Bragg reflection peaks, revealing thus their presence might support the GNPs' stability.

3.2. 2 Scanning Electron Microscopy with Field Emission (FE-SEM)

As illustrated size in Fig. (3), the GNPs emerged as smooth structures with excellent separation and a spherical form with an average of 24.57 ± 2.51 nm with the corresponding size distribution. Most of the particles exhibited a single, homogeneous distribution with no aggregations. This could be attributed to the GNPs being citrate reduced solution. Citrate ions can offer a negative charge on the GNP's surface, allowing them to easily disperse (10). GNPs made up of different elements, determined using EDX analysis, it contains data on the qualitative and quantitative states of materials that might be involved in the creation of GNPs. The existence of elemental gold (Au) in the sample was established by the EDX image's distinctive peaks, with the highest concentration assessed (1 mμ mL^{-1}). Other elements detected by EDX in the sample included O and Cl, which were mostly related to the HAu.Cl4.3H2O structure. The presence of Na and C can be attributed to the use of sodium citrate in the reduction of gold salts to GNPs.results, on the other hand, the presence of elemental gold (Au) was verified, indicating the stability of the GNPs with the functionalization process. The presence of Al can be attributed to the aluminum EDX plate used to analyze the sample.

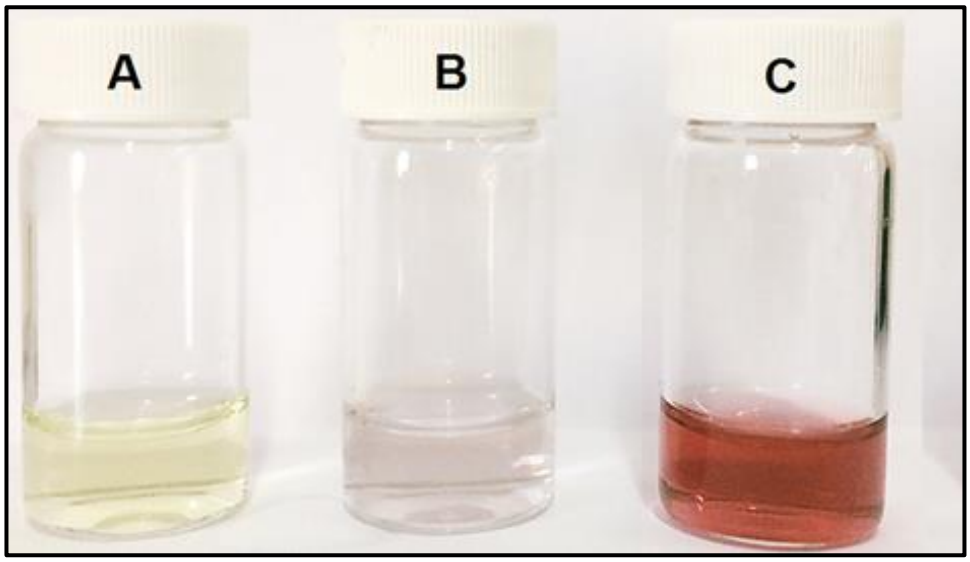

Figure 1: Preparation of gold nanoparticles. Suspensions of gold salt solution (A), gold nanoparticles of large size (B), and gold nanoparticles of optimal size (C).

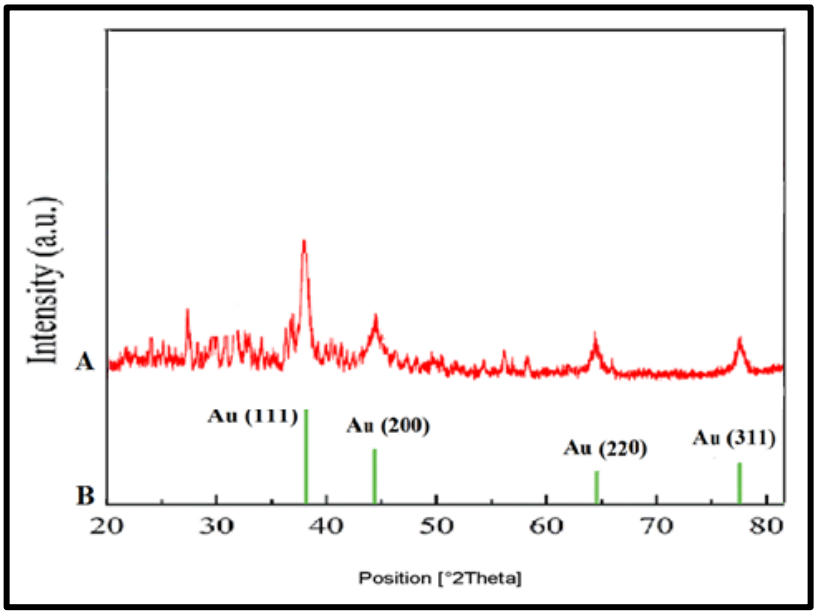

Figure 3: The XRD patterns of (A) and (B) Au (JCPDS file: 04-0784) gold electrodeposits obtained from the introduced cyanide-free gold electroplating electrolyte.

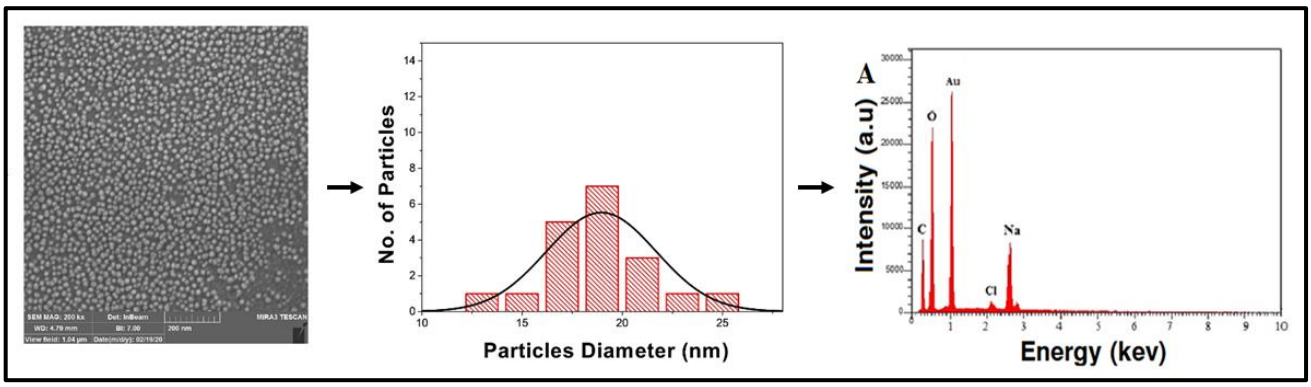

Figure 3: Scanning electron microscopic images for GNPs with their corresponding particle size distribution histogram and **EDX image.**

3.2.3 Transmission Electron Microscopy (TEM)

The form and distribution of the GNPs were validated using TEM imaging (Fig. 4). The average diameter of GNPs obtained through TEM image analysis was 24.32 ± 1.32 nm. The size diameter of GNPs was generally similar to that of GNPs with a citrate coating. This is owing to the low electrical density of the polymer and peptide layers, which made them hardly visible under electron microscopy (11). The particles were hexagonal, triangular, pentagonal, and spherical, with the common being spherical. That it is evident the material containing PEG's complex functional groups plays a significant role in the production of various nanoparticle morphologies (12). As a result, the specific interaction of the PEG to the GNPs at dissimilar surfaces led to different conjugate forms.

Cell-based high content screening (HCS) is considered to be a more predictive assay compared with conventional cytotoxicity assays. It covers a broad range of effects, monitoring multiple and independent toxicities in the same cell with a quantitative measurement of many parameters related to toxicity (13). Therefore, the cytotoxicity of GNPs in MCF7 cells over 24 hrs was evaluated by HCS. A treatment of 100 µg mL^{-1} of GNPs was used to detect changes in MCF7 cell viability, nuclear intensity, membrane permeability, mitochondrial membrane permeability, and cytochrome C. Results in Table (1), show the mean changes in florescent intensity regarding these 5 parameters. The significant changes (*p*-value) in these parameters were obtained by comparing with doxorubicin (1 mM) as a positive control and untreated cells as a negative control. Images of treatments with GNPs, doxorubicin, and untreated MCF-7 cells have resulted in Fig. (5).

3.3 High-Content Screening (HCS) Assay

Cell-based high content screening (HCS) is considered to be a more predictive assay compared with conventional cytotoxicity assays. It covers a broad range of effects, monitoring multiple and independent toxicities in the same cell with a quantitative measurement of many parameters related to toxicity (13). Therefore, the cytotoxicity of GNPs in MCF7 cells over 24 hrs was evaluated by HCS. A treatment of 100 µg mL^{-1} of GNPs was used to detect changes in MCF7 cell viability, nuclear intensity, membrane permeability, mitochondrial membrane permeability, and cytochrome C. Results in Table (1), show the mean changes in florescent intensity regarding these 5 parameters. The significant changes (*p*-value) in these parameters were obtained by comparing with doxorubicin (1 mM) as a positive control and untreated cells as a negative control. Images of treatments with GNPs, doxorubicin, and untreated MCF-7 cells have resulted in Fig. (5).

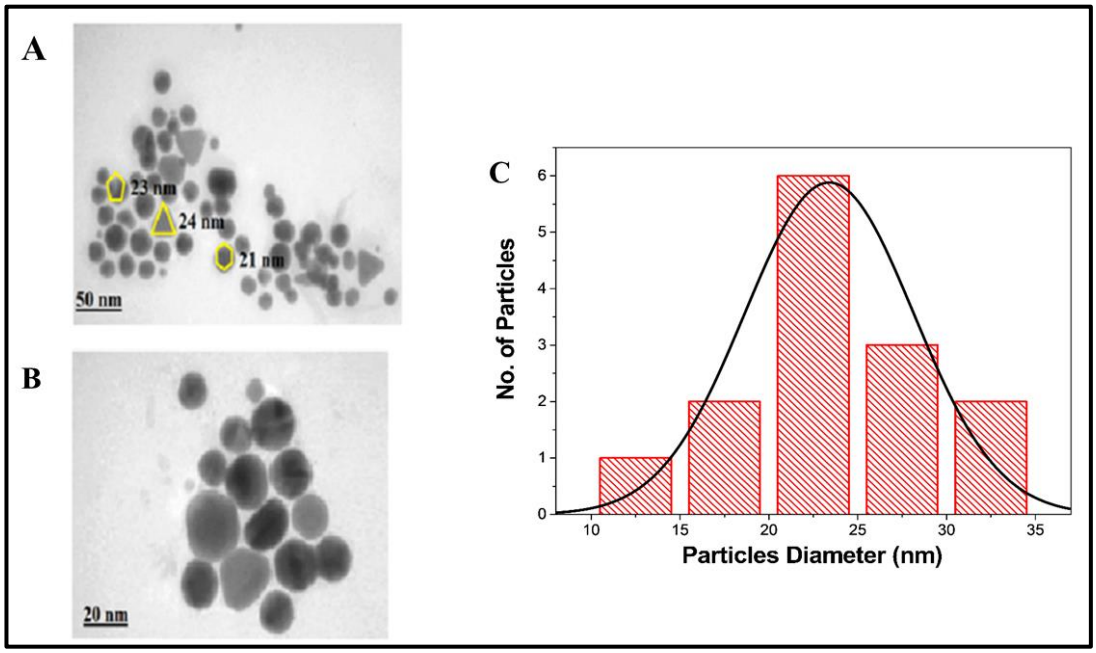

Figure 4: Transmission electron microscopy analysis of GNPs with different diameters and shapes at 50 nm scale (A) and 20 nm scale (B) together with the histogram of the particle size distribution (C).

Table 1: Cytotoxic effects of GNPs on cellular parameters by HCS.

VCC: Viable Cell Count; **TNI**: Total Nuclear Intensity; **MMP**: Mitochondrial Membrane Potential; **CMP**: Cell Membrane Permeability; **CC**: Cytochrome C. Letters (a, b and c) are significant at $p \leq 0.05$.

Treatment (100 µg mL^{-1})	**HCS Parameter (mean ± SD)**				
	VCC	**TNI**	**CMP**	**MMP**	**C C**
Untreated Cells	4065 ± 269.4^{a}	427.5 ± 58.69^{a}	149.5 ± 20.51^{a}	729.5± 16.26^{a}	400.5 ± 20.51^{a}
Doxorubicin 1mM	3073 ± 251.0^{b}	725.5 ± 50.20^{c}	316.5 ± 17.68^{c}	359.5± 44.55^{c}	552.0 ± 14.14^{b}
GNPs	2930 ± 255.3^{c}	659.5± 43.13^{b}	281.5 ± 3.536^{b}	491.0 ± 53.74^{b}	572.5 ± 12.02^{b}

3.3.1 The Viable Count

Results in Fig. (6) show that the viable count of MCF-7 cells was significantly decreased (p = 0.0085) when treated with 100 µg mL^{-1} of GNPs as compared with untreated cells. Cell viability is an important toxicity assay parameter and is directly associated with the toxic effects of a drug (14). The reduction of MCF-7 cells by GNPs was found to result from the effects of GNPs which increased the bioavailability of compounds in target cells. Such effects may be accredited to cytostatic and/or cytocide effects that might down-regulate telomerase activity (15).

3.3.2 Total Nuclear Intensity

Treatment of MCF-7 cells with the GNPs increased the size of the nucleus which is attributed to nuclear swelling. Nuclei stained with Hoechst blue appeared to be mostly condensed in response to the treatment with the GNPs at IC_{50} concentration (1.5-fold increase in nuclear fluorescence intensity), with significant differences (p < 0.0263) as compared to the cells without treatment (Fig. 7). The condensed and bright intensity of Hoechst blue stain was contributed to the nuclear condensation and such observations are the typical features of apoptotic cell morphology: nuclear condensation, nuclear fragmentation, cell shrinkage, formation and aggregation of apoptotic bodies (16). The results also demonstrated that the mitochondrial membrane of the MCF-7 was more permeable following treatment with the conjugate. This treatment has possibly caused changes in the mitochondrial function which led to cell death either by necrosis or apoptosis. These events can cause the mitochondrial membrane to lose its potential with the subsequent release of cytochrome C.

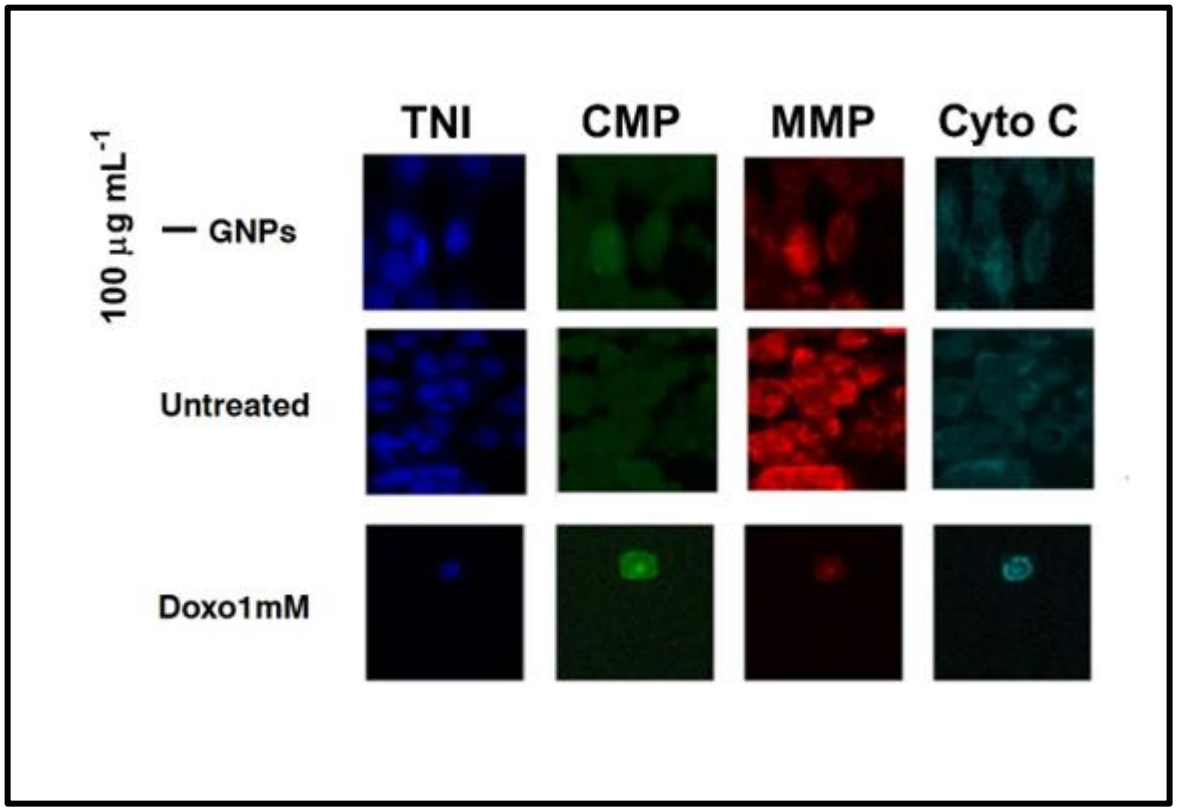

Figure 5: Multiparameter cytotoxic analysis of MCF-7 cells treated with 100 µg mL^{-1} of GNPs after 24hrs of incubation at 37ºC. Cells were stained with Hoechst 33342 (Blue) (*Ex* 330 nm / *Em* 420 nm) Dye which enables monitoring of cell loss, nuclear morphology changes, and DNA content, Permeability Dye (Green) (*Ex* 491nm /*Em* 509 nm) for membrane permeability monitoring, MMP Dye (Red) (*Ex*552 nm /*Em* 576 nm) for mitochondrial membrane potential changes, and with goat anti-mouse, secondary antibody conjugated with DyLight™ for Cytochrome C releasing.

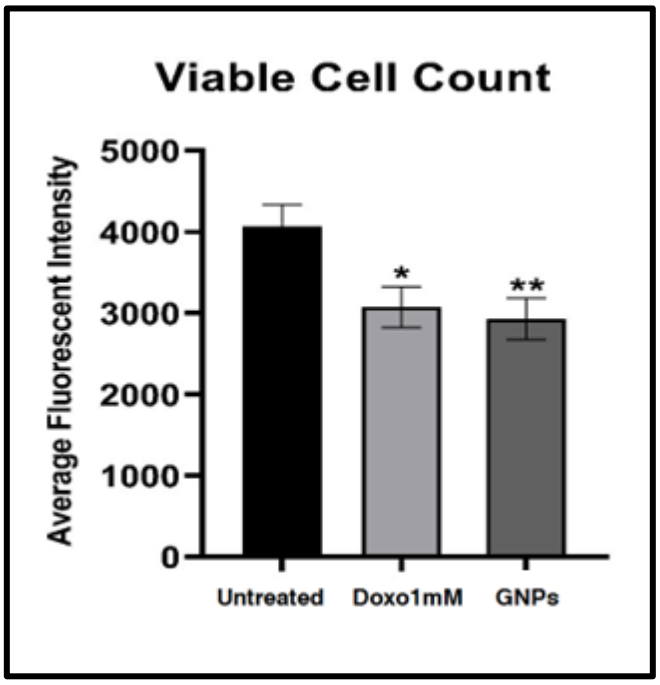

Figure 6: Reduction in MCF-7 cell count after 24 hrs exposure to GNPs at 37°C and evaluated on the Array Scan HCS Reader, mean (±SD) differences for significance were made between the untreated cells and the whole group. **: $p \leq 0.01$, *: $p \leq 0.05$, NS: Non-Significant, SD: Standard Deviation, $n = 3$.

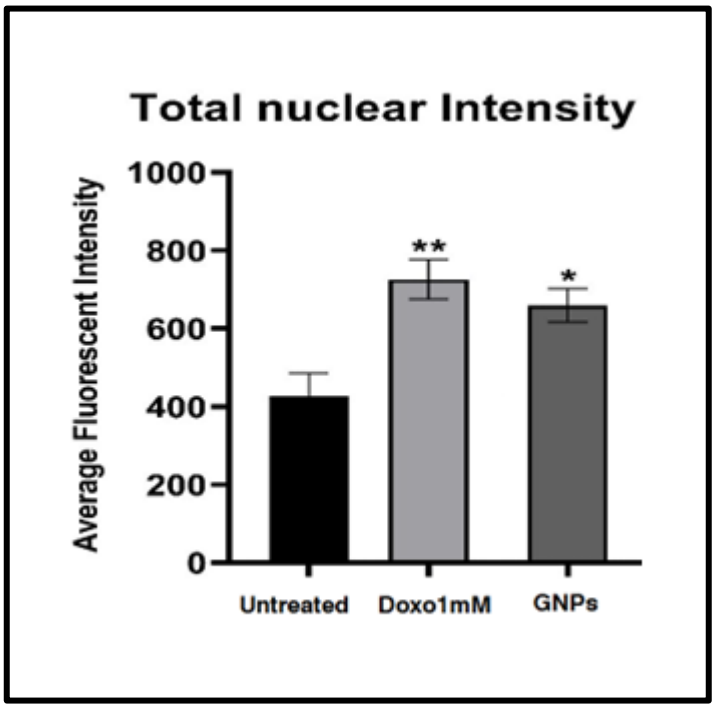

Figure 7: Mean (±SD) effect of GNPs treatment on total nuclear intensity in MCF-7 after 24 hrs at 37°C. The effect was evaluated on the Array Scan HCS Reader, and mean differences for significance were made between the untreated cells and the whole group. **: $p \leq 0.01$, *: $p \leq 0.05$, NS: Non-Significant, SD: Standard Deviation, $n = 3$.

3.3.3 Cell Membrane Permeability

Cell membrane permeability is often linked to a toxic or apoptotic response, and the damage to cell membrane integrity is a common phenotypic feature of marked cytotoxicity (17). As shown in Fig. (8), GNPs treatment exhibited the maximum significant (p = 0.0019) increase in membrane permeability compared with untreated cells. The results support the notion that the GNPs induced apoptosis of cancer cells, as indicated by the increased plasma membrane permeability to the dye. These effects are typically observed when the plasma membrane loses its integrity, with various cell death mechanisms inducing specific reshuffling events in the plasma membrane (18). GNPs may change both the structure and organization of lipids forming the intracellular as well as the plasma membranes. These events can alter the permeability in response to a second messenger mechanism via the phospholipase pathway associated with continuous activation of protein kinase C. Such mechanisms can affect the cell's normal function and then lead to cell lysis (19).

3.3.4 Mitochondrial Membrane Potential (MPP)

The MMP dye was utilized to determine the functionality of the active mitochondria due to its capability of accumulation within this organelle that maintains its inner membrane potential (20). For better characterization of cell death signaling pathways upon the toxicity of MCF-7cells, the effect of the GNPs as revealed in Fig. (9), GNPs induced a significant (p = 0.0053) decrease in MMP by 32.7%, whereas the positive control showed a decrease of 50.8%, in comparison to the untreated cancer cells. MPP measurement was based on the mean intensity of MMP dye penetrating the mitochondria; the less fluorescent intensity the highest effect on the mitochondria caused. During cancer development, apoptosis is often dysregulated. In the majority of cases, triggering of proper apoptosis occurs via the mitochondrial outer membrane permeabilization (MOMP), which delineates the mitochondrial (i.e. intrinsic) pathway and eventually results in caspase activation and protein substrate cleavage. This pathway of apoptosis is initiated by the MOMP (21).

3.3.5 Cytochrome C Release

Cytochrome C has a remarkable role in apoptosis, during which it is released from the mitochondria into the cytoplasm, resulting in the activation of the caspase cascade and thereby the commitment of the cell to the death pathway. It was suggested that the release of cytochrome C is a result of the swelling of the mitochondrial matrix which is in turn initiated by the apoptotic stimuli (22). Results demonstrate that Cytochrome C stained weakly and diffusely in the control cells. In contrast, the GNPs treated MCF-7 cells showed distinguished staining around the nucleus significantly (p = 0.0016) inducing the release of cytochrome C (0.43-fold increased mean intensity), (Fig. 10). This finding proposes that cytochrome C was translocated in higher levels from the mitochondria into the cytosol upon treatment with the GNPs. Infrequently, cytochrome C was present within the nuclei of GNPs treated cells, whereas the control cells did not show such an effect. When released, cytochrome C leads to the activation of a cascade of caspase and cysteine proteases, which are the main players in the events of the degradation and digestion of the cell from inside (23).

Conclusion

GNPs were successfully synthesized and characterized quantitatively and qualitatively by using FE-SEM, XRD, and FEM. Several cellular parameters (such as cell viability, membrane permeability, mitochondria membrane permeability, cytochrome c, and nuclear intensity) were measured via the HCSA system. From the combined quantitative HCSA analysis at 24 h exposure for GNPs, overall, these results suggest that GNPs may cause cell death in MCF7 cells by inducing the mitochondrial membrane permeability change which leads to cytochrome c release which leads to apoptotic cell death.

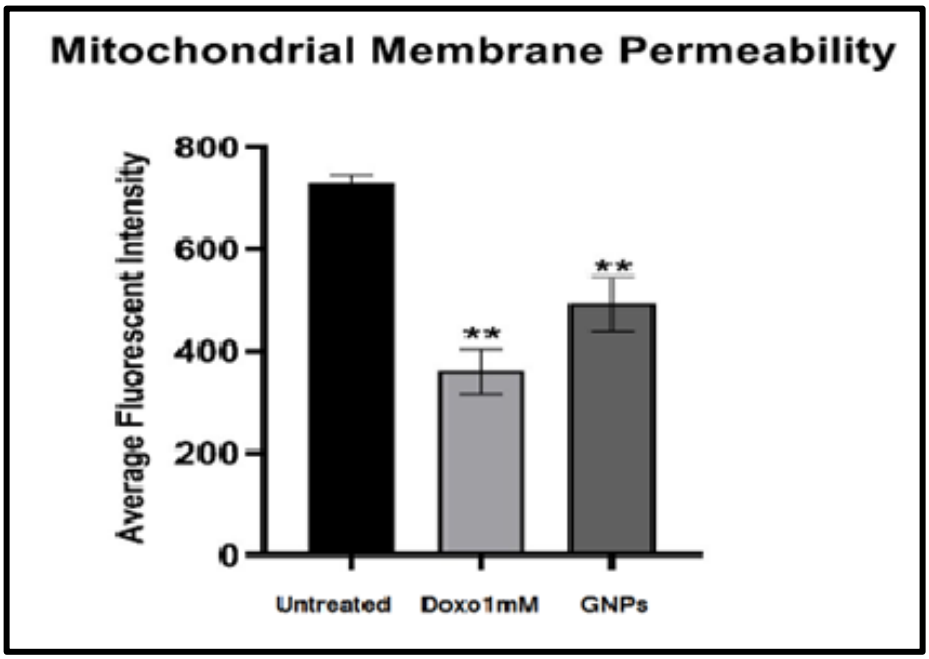

Figure 8: Mean (±SD) effect of GNPs treatment on cell membrane permeability in MCF-7 after 24 hrs at 37°C. The effect was evaluated on the Array Scan HCS Reader, and mean differences for significance were made between the untreated cells and the whole group. **: $p \leq 0.01$, NS: Non-Significant, SD: Standard Deviation, n = 3.

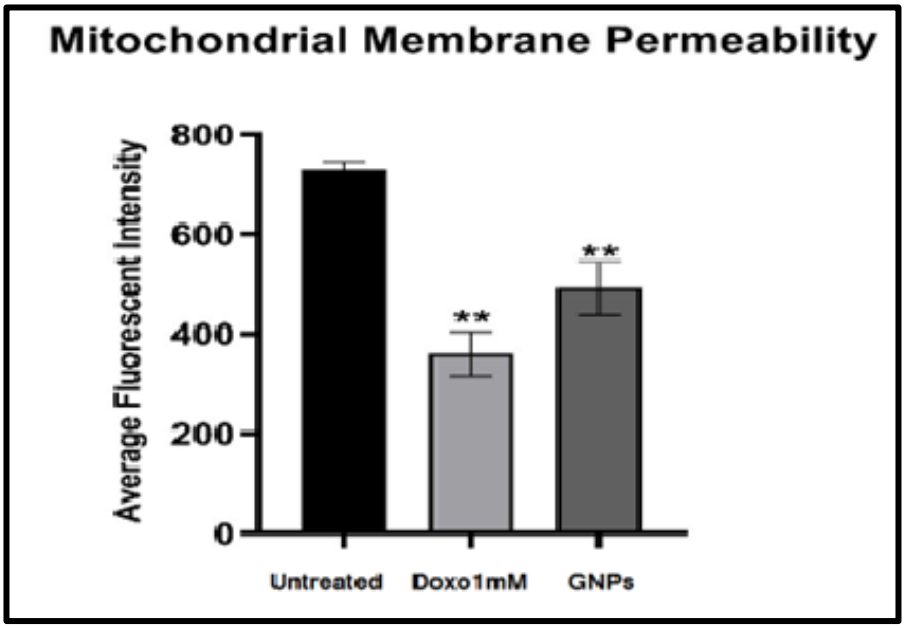

Figure 9: Mean (±SD) effect of GNPs treatment on mitochondrial membrane permeability in MCF-7 after 24 hrs at 37°C. The effect was evaluated on the Array Scan HCS Reader, and mean differences for significance were made between the untreated cells and the whole group. **: $p \leq 0.01$, NS: Non-Significant, SD: Standard Deviation, n = 3.

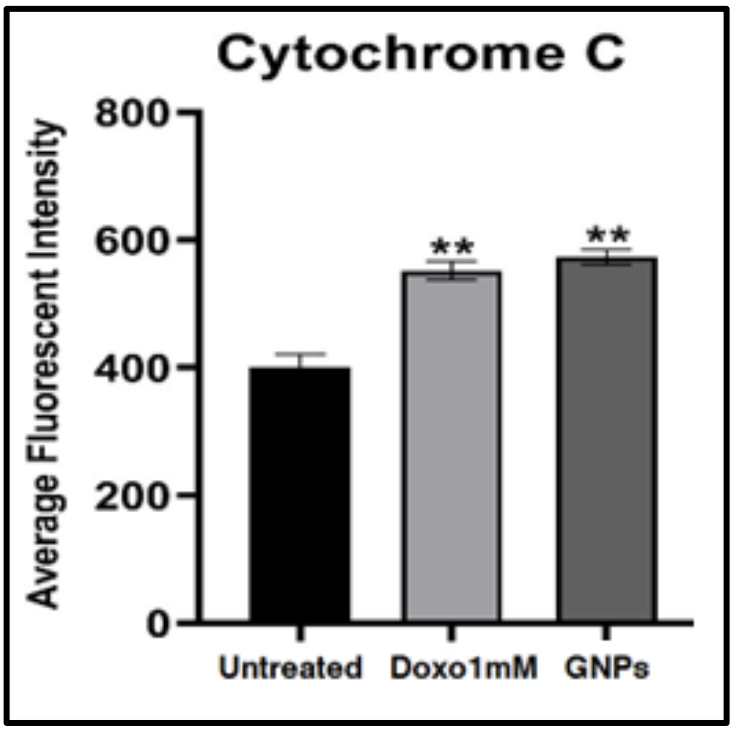

Figure 10: Mean (±SD) effect of GNPs treatment on cytochrome C release in MCF-7 after 24 hrs at 37°C. The effect was evaluated on the Array Scan HCS Reader, and mean differences for significance were made between the untreated cells and the whole group. **: $p \leq 0.01$, NS: Non-Significant, SD: Standard Deviation, $n = 3$.

References

1. Siegel, R.L.; Miller, K.D.; Goding Sauer, A.; Fedewa, S.A.; Butterly, L.F.; Anderson, J.C.; Cercek, A.; Smith, R.A.and Jemal, A. (2020). Colorectal cancer statistics, 2020. CA: A Cancer Journal for Clinicians
2. Mitra, A.K.; Agrahari, V.; Mandal, A.; Cholkar, K.; Natarajan, C.; Shah, S.; Joseph, M.; Trinh, H.M.; Vaishya, R.and Yang, X. (2015). Novel delivery approaches for cancer therapeutics. Journal of Controlled Release 219 248-268.
3. Graczyk, A.; Pawlowska, R.; Jedrzejczyk, D.and Chworos, A. (2020). Gold nanoparticles in conjunction with nucleic acids as a modern molecular system for cellular delivery. Molecules 25 (1): 204.
4. Sotnikov, D.V.; Berlina, A.N.; Ivanov, V.S.; Zherdev, A.V.and Dzantiev, B.B. (2019). Adsorption of proteins on gold nanoparticles: One or more layers. Colloids and Surfaces B: Biointerfaces 173: 557-563.
5. Al-Dulimi, Ali G., Ali Z. Al-Saffar, and Ghassan M. Sulaiman. "Enhanced cellular uptake and anti-cancer potentials of gold nanoparticles conjugated with cell penetration peptide against lung cancer cells." *IOP Conference Series: Materials Science and Engineering*. Vol. 928. No. 6. IOP Publishing, 2020.

6. Al-Dulimi, Ali G., et al. "Immobilization of l-asparaginase on gold nanoparticles for novel drug delivery approach as anti-cancer agent against human breast carcinoma cells." *Journal of Materials Research and Technology* 9.6 (2020): 15394-15411.

7. Lingling, W.; Guihua, Z.; Wei, Y.; Dahai, Z.; Yingchun, Z.; Liye, Z.and Huaqing, X. (2018). Photothermal properties of near-spherical gold nanofluids with strong localized surface plasmon resonance. *Journal of Thermal Science and Engineering Applications* 10 (1).

8. Vijayakumar, S.; Vaseeharan, B.; Malaikozhundan, B.; Gopi, N.; Ekambaram, P.; Pachaiappan, R.; Velusamy, P.; Murugan, K.; Benelli, G.and Kumar, R.S. (2017). Therapeutic effects of gold nanoparticles synthesized using Musa paradisiaca peel extract against multiple antibiotic resistant Enterococcus faecalis biofilms and human lung cancer cells (A549). *Microbial Pathogenesis* 102 173-183.

9. Kong, F.-Y.; Zhang, J.-W.; Li, R.-F.; Wang, Z.-X.; Wang, W.-J.and Wang, W. (2017). Unique roles of gold nanoparticles in drug delivery, targeting and imaging applications. *Molecules* 22 (9): 1445.

10. Crowley, L.C.; Marfell, B.J.and Waterhouse, N.J. (2016). Analyzing cell death by nuclear staining with Hoechst 33342. *Cold Spring Harbor Protocols* 2016 (9): pdb. prot087205.

11. Bachelet, M. (2017). Synthesis, physicochemical characterization and biological evaluation of polymer-functionalized gold nanoparticles for cancer treatment. *Imperial College London*, PhD theses.

12. Premkumar, T.; Lee, K.and Geckeler, K.E. (2011). Shape-tailoring of gold nanostructures: can a detergent act as the reducing or protecting agent. *Nanoscale* 3 (4): 1482-1484.

13. O'Brien, P.J.and Edvardsson, A. (2017). Validation of a multiparametric, high content-screening assay for predictive/investigative cytotoxicity: evidence from technology transfer studies and literature review. Chemical Research in Toxicology 30 (3): 804-829

14. Al-Jailawi, M.; Nasir, H.and Aziz, G. (2015). Cytotoxic effect of biosurfactants produced by novel thermophilic Geobacillus thermoleovorans (JQ 912239). Int J Adv Res 3 632-637.

15. Ajabnoor, G.; Crook, T.and Coley, H.M. (2012). Paclitaxel resistance is associated with switch from apoptotic to autophagic cell death in MCF-7 breast cancer cells. Cell Death & Disease 3 (1): e260-e260.

16. Crowley, L.C.; Marfell, B.J.and Waterhouse, N.J. (2016). Analyzing cell death by nuclear staining with Hoechst 33342. Cold Spring Harbor Protocols 2016 (9): pdb. prot087205

17. Al-Saily, H.M.; Al-Halbosiy, M.M.and Al-Hady, F.N. (2019). Cytotoxic and apoptotic effects of cyproterone acetate against cancer cells and normal cells. Journal of Biotechnology Research Center 13 (1): 68-74.

18. Zhang, Y.; Chen, X.; Gueydan, C.and Han, J. (2018). Plasma membrane changes during programmed cell deaths. Cell Research 28 (1): 9-21.

19. Khadka, N.K.; Cheng, X.; Ho, C.S.; Katsaras, J.and Pan, J. (2015). Interactions of the anticancer drug tamoxifen with lipid

membranes. Biophysical Journal 108 (10): 2492-2501.

20. Seki, H.; Onishi, S.; Asamura, N.; Suzuki, Y.; Kawamata, J.; Kaneno, D.; Hadano, S.; Watanabe, S.and Niko, Y. (2018). Bright and two-photon active red fluorescent dyes that selectively move back and forth between the 141 References mitochondria and nucleus upon changing the mitochondrial membrane potential. Journal of Materials Chemistry B 6 (45): 7396-7401.
21. Kalkavan, H.and Green, D.R. (2018). MOMP, cell suicide as a BCL-2 family business. Cell Death and Differentiation 25 (1): 46-55.
22. Alvarez-Paggi, D.n.; Hannibal, L.; Castro, M.A.; Oviedo-Rouco, S.; Demicheli, V.; Tórtora, V.;Tomasina, F.; Radi, R.and Murgida, D.H. (2017). Multifunctional cytochrome c: learning new tricks from an old dog. Chemical Reviews 117 (21): 13382-13460.
23. Al-Shukri, A.F.; Al-Marzook, F.A.; Al-Hammadi, N.A.and Mutlag, I.H. (2020). Antitumor Activity of Alkaloids Extract from Opuntia polyacantha Plant Using High Content Screening Technique. Pharmacophore 11(1): 129-135.
24. Ahmed F. Hasan, Thulfiqar F. Mutar, Ehab Moustafa Tousson and Shatha Ghazi Felemban. (2021). Therapeutic Effects of Turnera diffusa Extract Against Amitriptyline-Induced Toxic Hepatic Inflammation. OnLine Journal of Biological Sciences (2):, 21: 395.408.